Korean J. Chem. Eng., 39(8), 2117-2126 (2022)
DOI: 10.1007/s11814-022-1180-6

pISSN: 0256-1115
eISSN: 1975-7220

Adsorption behavior of phosphate on 2-L ferrihydrite adsorbent predicted by partial charge model under varying pH conditions

Seung-Joon Yoo†

Resources Development Research Institute, Department of Earth Resources and Environmental Engineering, Hanyang University, 222 Wangsimni-ro, Seongdong-gu, Seoul 04763, Korea
(*Received 15 October 2021 • Revised 10 May 2022 • Accepted 14 May 2022*)

Abstract−The surface charge of the adsorbent 2-L ferrihydrite was calculated by the partial charge model for varying pH conditions. The value of the surface charge was used to predict the ability of the adsorbent to chemically adsorb and desorb the adsorbate. The crystal structure of the 2-L ferrihydrite material was regarded as two models: an exclusively octahedral model and a combined model comprising 20% tetrahedra and 80% octahedra. The partial charge model was used to calculate the surface charge of the adsorbent under varying pH conditions. In the exclusively octahedral model, the surface charge reached the highest value of +0.060 under acidic conditions, −0.088 in the neutral state, and the lowest value of −0.347 under alkaline conditions. In the case of the combined model, δ(OH) had the highest value of +0.056 under acidic conditions, −0.087 in the neutral state, and the lowest value of −0.332 under alkaline conditions. As a result, we confirmed that the surface charge of the adsorbent could have a positive value even in an acidic environment. That is, the surface charge of the adsorbent could become positive or negative according to the pH of the solution. In a solution in which the pH is below 10, the adsorbent could adsorb the negative phosphate because the δ(OH) would be positive. In contrast, in a solution with pH>10, the adsorbent could desorb the negative phosphate because the δ(OH) would be negative.

Keywords: Partial Charge Model, 2-L Ferrihydrite Adsorbent, Phosphate Adsorbate, Surface Charge, Adsorption, Desorption

INTRODUCTION

The prevention of the eutrophication of water has led to the use of many adsorbents for the removal of phosphate ions, which are well-known to be a major factor responsible for promoting algal growth. Among them, recently proposed adsorbents such as Ca-enriched biochar [1], MgO modified dilatomite [2], a 3D graphene-La_2O_3 composite [3], a 3D graphene/$La(OH)_3$ nanorod aerogel [4], nanoscale lanthanum carbonate [5] and mesoporous silica aerogels impregnated with La [6], have increased the phosphate adsorption efficiency and maximum adsorption capacity, as shown in Table 1.

In this study, we chose iron oxyhydroxide as the adsorbent material because of its excellent performance compared with the various adsorbents described above. In addition, iron oxyhydroxide has been widely used as the adsorbent for water remediation as an objective adsorbent.

Iron oxyhydroxides and -oxides have various transitional structures, i.e., α-, β-, γ-, δ-, ε-, feroxyhite, and ferrihydrite, as presented in Fig. 1. Depending on the treatment temperature, these transitional structures are determined by the amount of adsorbed water and the structural water included in the crystal structure. Among these iron oxyhydroxides and -oxides, 2-L ferrihydrite has widely been used as one of the most important mineral adsor-

Table 1. Efficiency of phosphate removal for various adsorbents

Adsorbent	Surface area (m^2/g)	Adsorbent dosage (g/L)	Max. adsorption capacity (mg/g)	Initial phosphate conc. (mg/L)	pH/ T (K)	Ref.
Ca-enriched biochar	4.74	0.5	146.33	100	8/298	[8]
MgO modified dilatomite	45.17	0.3	104.94	120	3/298	[9]
3D graphene-La_2O_3 composite	197.18	2	82.6	25	6.2	[10]
3D graphene/$La(OH)_3$ nanorod aerogel	180.8	0.25 g	76.85	2	298	[11]
Nanoscale lanthanum carbonate	19.63	0.1	53.64	2-50	6.8/303	[12]
Mesoporous silica aerogels impregnated La	262.69	1	42.08	200	3/298	[13]

†To whom correspondence should be addressed.
E-mail: sjyoo001@hanyang.ac.kr
Copyright by The Korean Institute of Chemical Engineers.

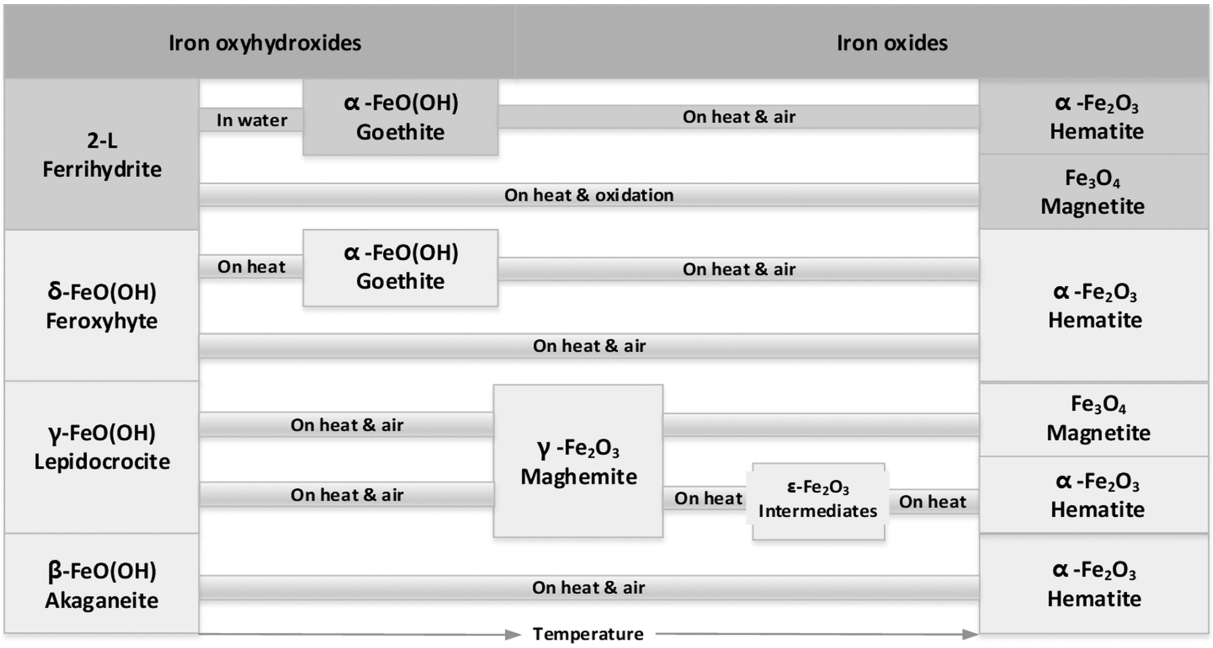

Fig. 1. Sequence of transitional iron oxyhydroxides and oxides [25].

bents. This adsorbent forms strong complexes with various cations and anions, such as cadmium(II) [7,8], chromate(VI) [9,10], lead(II) and copper(II) [11], arsenic [12], and phosphate [13], because of its large surface area, high surface activity, and its affordability owing to its natural abundance.

2-L ferrihydrite is metastable [14] with an octahedral structure as a rule. However, various hypotheses have led to the proposal of the definite crystal structure, depending on the presence or absence of tetrahedral Fe^{3+} [15-24].

Recent research proposed that the adsorption of an adsorbate onto an adsorbent is governed by the hydroxyl groups on the surface [26,27]. Thus far, a partial charge model has been used to predict the surface charge [28-33]. The prediction of the adsorption behavior by the calculation of the surface charge is a good method for the explanation of the phenomenon of chemical adsorption.

The concept of the partial charge model is based on the following. When two components are bound, electron transport occurs between them owing to the difference in the electronegativity of the two elements. Electron transfer proceeds until the chemical potentials attain equilibrium and the electrons in the compound are redistributed. Then, the electronegativity of the two components in the compound finally reaches equalization. That is, the key aspect of the partial charge model is that the surface charge of an atom is highly influenced by the surrounding atoms. The partial charge of an atom in the adsorbent can be calculated using the partial charge model, and the value determines the transport velocity of electrons and the adsorption ability.

Electronegativity is the electronic chemical potential, and the equalization of the electronegativity thermodynamically corresponds to the equalization of the chemical potential in the state of equilibrium.

The electronegativity, χ_i of an atom is not constant, and it varies with the partial charge of the atom, δ_i. Commonly, it is assumed to change linearly with its charge [33,34].

$$\chi_i = \chi_i^o + \eta_i \delta_i \tag{1}$$

where χ_i is the electronegativity of the i atom, and χ_i^o is the electronegativity of the neutral atom, δ_i is the partial charge of the i atom, and η_i corresponds to the "hardness" in the Pearson's model [35], which may be defined as:

$$\eta_i = \mathrm{k}\sqrt{\chi_i^o} \tag{2}$$

where k is a constant that depends on the electronegativity scale (k=1.36 for Pauling's scale). According to the principles of electronegativity equalization by Sanderson, charge transfer is expected to cease when the electronegativities of all constituent atoms become equal to the mean electronegativity $\overline{\chi}$ given by:

$$\overline{\chi} = \frac{\Sigma \mathrm{p}_i \sqrt{\chi_i^o} + \mathrm{kZ}}{\Sigma \mathrm{p}_i / \sqrt{\chi_i^o}} \tag{3}$$

The electronegativity corresponds to the electronic chemical potential and electronegativity equalization in the equilibrium state.

The total charge conservation follows from

$$\mathrm{Z} = \Sigma \mathrm{p}_i \delta_i \tag{4}$$

where Z is the total charge of the ionic species and p_i corresponds to the stoichiometry of the i atom in the compound.

For a diatomic molecule AB, the mean electronegativity actually corresponds to the geometric mean of both electronegativities:

$$\overline{\chi}_{AB}^o = \sqrt{\chi_A^o \cdot \chi_B^o} \tag{5}$$

The partial charge distribution is given by:

$$\delta_i = \frac{\overline{\chi} - \chi_i^o}{\mathrm{k}\sqrt{\chi_i^o}} \tag{6}$$

The surface charge of atom A or B is influenced by the surround-

ings of these atoms as well as the electronegativities of the two atoms A and B. In summary, the individual partial charge of atom A or B is not a fixed value and is affected by the other atoms in the compound and the solution condition containing atoms A and B [32].

Under acidic condition, the adsorbed water and the structural water included in the crystal structure of the 2-L ferrihydrite adsorbent are replaced by H_3O^+ ions in the solution [36]. As a result, the surface charge of the adsorbent is increased. Contrary to this result, the surface charge decreases in a strongly alkaline solution.

1. Crystal Structure

During more than 40 years of investigation, researchers have proposed various structure models based on 2-L ferrihydrite material using refined characterization techniques [37-42]. However, the 2-L ferrihydrite with its low crystallinity and structural disorder basically has an octahedral structure, whereas the presence of tetrahedral Fe^{3+} is still under debate. Nonetheless, the most influential model is classified as two models for the formation of Fe-H_2O and Fe-OH bonds: In the first model, the crystal structure exclusively exists as an octahedral-coordinated structure. The second model has an iron Keggin structure. The structure consists of a central tetrahedral oxoanion FeO_4. Each of the four oxo bridges forms a trimer of edge-sharing FeO_6 octahedra, and the general framework contains iron-oxyhydroxide Keggin units [36]. In the structure of 2-L ferrihydrite, the central FeO_4 tetrahedra are surrounded by 12 FeO_6 octahedra [39-42].

Accordingly, we considered two models as the representative models: an exclusively octahedral structure and a combined structure that is the octahedral structure with a 20% tetrahedral structure.

EXPERIMENTAL

1. Materials and Methods

The 2-L ferrihydrite adsorbent was chosen as the target material in this experiment. The 2-L ferrihydrite was synthesized by dissolving iron waste scrap in H_2SO_4 (Merck, 95%) by heating the mixture for 8 hours at 70 °C and stirring at 400 rpm. Then, the ferric sulfate solution obtained after dissolution was simultaneously oxidized by aeration and the addition of hydrogen peroxide (H_2O_2, 30%, Merck) to induce the oxidation of Fe^{2+} to Fe^{3+} as shown in Fig. 2.

In the next step, the pH of the solution was controlled to pH 6.0 by adding sodium hydroxide (NaOH, 99%, Merck) to induce precipitation and crystallization. The 2-L ferrihydrite adsorbent was finally obtained through washing, centrifugal separation, and drying at 130 °C.

2. Adsorption Experiment

Adsorption experiment was carried out to measure the adsorption performance on the synthesized 2-L ferrihydrite adsorbent as shown in Fig. 3. The batch experiment was conducted by preparing phosphate stock solutions of 300 ppm by dissolving orthophosphoric acid (H_3PO_4, 85.00%, Merck) in deionized water. The phosphate solution was controlled to the pH range of 1 to 13. At this time, HCl or NaOH solution was added to the phosphate solution to adjust the pH to within the range of 1 to 13. All the batch experiments were carried out by placing equal amounts of the adsorbent (2.5 mg) in 10 mL phosphate solution using falcon tubes, which were then agitated for 24 h using a tube roller mixer.

3. Analysis

The metal composition of the iron waste scrap was analyzed by an inductively coupled plasma-mass spectrometer (ICP-MS, Agilent 7700s) with high sensitivity and accuracy by argon plasma source after the dissolution of the iron waste scraps in nitrohydrochloric acid.

The X-ray diffraction (XRD) patterns were recorded using an X-ray diffractometer (X'PERT-PRO MPD, Malvern PANalytical) equipped with a CuKα radiation source (λ=1.5406 Å) and generator settings of 30 mA and 40 kV.

The microstructures and the diffraction patterns were studied using transmission electron microscopy (TEM, Tecnai, THERMO FISHER SCIENTIFIC). The microscope was equipped with field emission guns and operated at 300 keV. In preparation for the TEM (SAED, selected area electron diffraction) measurement, the 2-L ferrihydrite material was milled to an average particle size of 200 nm by Planetary Micro Mill (PULVERISETTE 7 Premium, FRITSCH, Germany) with a grinding ball of zirconia. The particle size and distribution of the milled 2-L ferrihydrite were analyzed under the following condition (water solvent, two semiconductor lasers (Green (λ=532 nm, 7 mW), IR (λ=850 nm, 9 mW), measuring range 0.08-2,000 μm) by particle size analyzer (ANALYSETTE 22 MicroTec plus, FRITSCH, Germany).

Nitrogen adsorption and desorption were measured at 77 K using a Micromeritics (TristarII 3020) surface area and porosity analyzer. The sample was automatically degassed for 30 h in an N_2 environ-

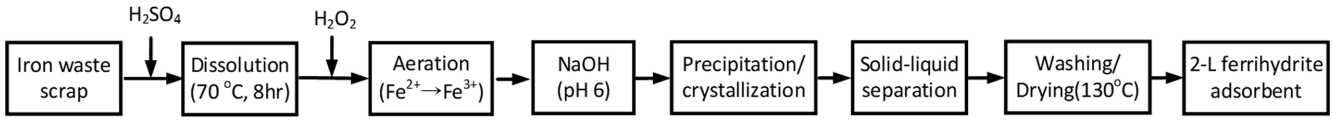

Fig. 2. Flow diagram for the preparation of the 2-L ferrihydrite adsorbent.

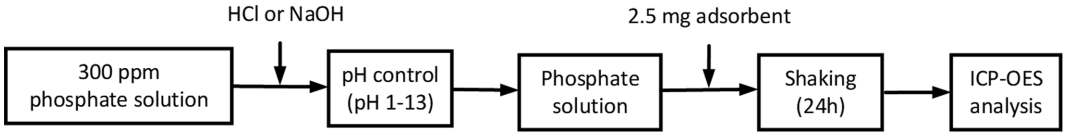

Fig. 3. Flow diagram for the phosphate adsorption experiment.

Table 2. Elemental compositions of iron waste scraps and 2-L ferrihydrite adsorbent analyzed by ICP-MS

Element	^{56}Fe (%)	^{24}Mg (%)	^{27}Al (%)	^{118}Sn (%)	^{66}Zn (%)	^{60}Ni (%)	^{52}Cr (%)	^{63}Cu (%)	^{47}Ti (%)
Iron waste scrap	64.09	1.13	0.26	0.13	0.07	0.08	0.01	0.11	0.02
2-L ferrihydrite adsorbent	98.84	0.04	0.15	0.03	0.26	0.04	0.01	0.05	0.01

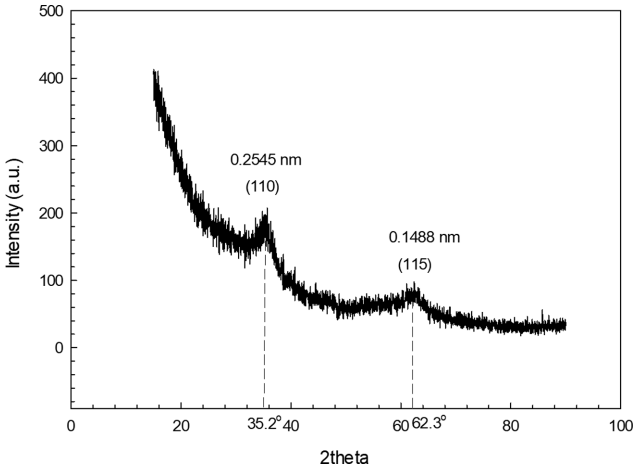

Fig. 4. XRD pattern of the 2-L ferrihydrite adsorbent.

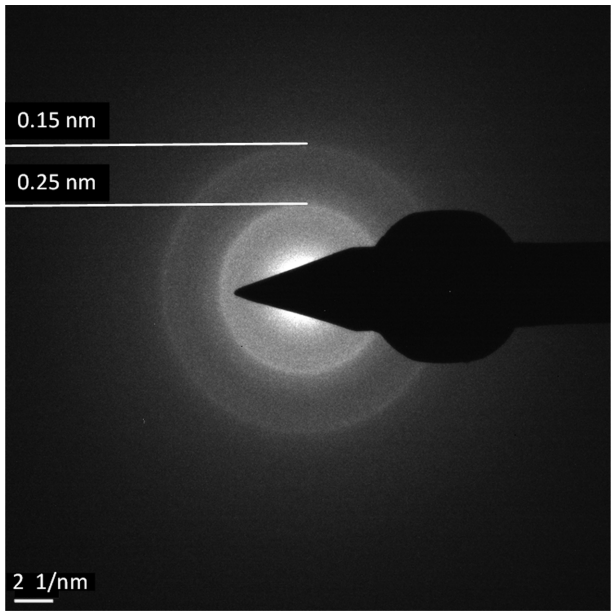

Fig. 5. SAED pattern of 2-L ferrihydrite with d-values of rings.

ment at 383 K in the degassing port of the adsorption apparatus.

The metal content of the adsorbent was analyzed using field-emission scanning electron microscopy (FE-SEM, HITACHI, SU8220) with EDS. The point of zero charge (PZC) of the 2-L ferrihydrite adsorbent was measured using an advanced electrochemistry meter (Orion VERSASTAR, Thermo Scientific). At this time, an amount of adsorbent corresponding to 1,000 m^2/L was constantly added to the solutions of which the initial pH values were adjusted from 1 to 13 by NaOH and HCl, respectively. Subsequently, we measured the final pH value after shaking these solutions for 10 hours using a tube roller mixer. The phosphate concentration of the adsorbent was analyzed by ICP-OES (iCAP6000 Series, Thermo Scientific, UK).

RESULTS AND DISCUSSION

The iron waste scrap was used as a raw material, considering economic and environmental resources recycling aspects. From the ICP-MS analysis of Table 2, the iron waste scrap had high iron content, including various impurities and metal oxides. The iron content of iron waste scrap was analyzed as 64.09%. On the other hand, the 2-L ferrihydrite showed relatively high iron content. The iron content of the 2-L ferrihydrite adsorbent synthesized from the experiment was 98.84%.

Fig. 4 shows the XRD pattern of the 2-L ferrihydrite adsorbent synthesized from iron waste scraps for this experiment. The adsorbent has a metastable structure with low crystallinity and has the typical XRD pattern (JCPDS card number 29-0712) of 2-L ferrihydrite with the characteristic broad bands at 35.2° and 62.3°, assigned to the (110) and (115) planes, respectively. The d-spacing of the (110) and (115) planes was 2.545 Å and 1.488 Å, respectively, as shown in Fig. 4. Other researchers proposed the same results on the basis of the XRD pattern [17,43-45]. Accordingly, the adsorbent is referred to as metastable 2-L ferrihydrite as a result of the two broad peaks.

SAED was used to examine the structure of the 2-L ferrihydrite materials. The SAED pattern, shown in Fig. 5, has two bright rings with two interplanar distances of 1.50 and 2.50 Å as proposed previously [43,45-48]. The measured d-spacings of the 2-L ferrihydrite were in agreement with those calculated from the XRD results.

Table 3 presents the result of the N_2 adsorption and desorption analysis of the 2-L ferrihydrite adsorbent before and after phosphate

Table 3. Physical properties of the 2-L ferrihydrite adsorbent

Property	Unit	2-L ferrihydrite adsorbent before phosphate adsorption	2-L ferrihydrite adsorbent after phosphate adsorption
BET surface area	m^2/g	237	235
Total pore volume	cm^3/g	0.175	0.175
Average pore size	nm	2.998	2.942

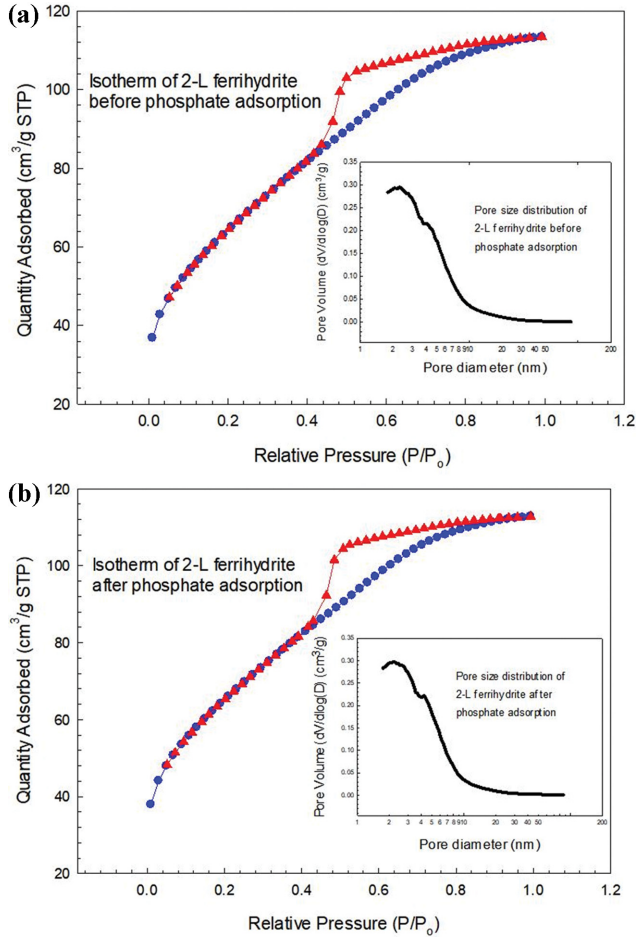

Fig. 6. Isotherms and pore size distributions of the 2-L ferrihydrite adsorbent: (a) before phosphate adsorption (b) after phosphate adsorption.

adsorption. The adsorbent had a BET surface area of 237 m^2/g, a total pore volume of 0.175 cm^3/g, and an average pore diameter of 2.998 nm before phosphate adsorption. After phosphate adsorption, the adsorbent had a BET surface area of 235 m^2/g, total pore volume of 0.175 cm^3/g, and average pore diameter of 2.942 nm, respectively.

Fig. 6(a) and (b) show the N_2 adsorption-desorption isotherm and pore size distribution of the 2-L ferrihydrite adsorbent before and after phosphate adsorption. The N_2 adsorption-desorption isotherm of the 2-L ferrihydrite exhibits type IV uptake as defined by the International Union of Pure and Applied Chemistry (IUPAC), characterized by a hysteresis loop after capillary condensation. Furthermore, type IV is characterized as a mesoporous adsorbent with strong adsorption affinity by a new classification of adsorption isotherms based on the Gibbs adsorption behavior [49]. From this result, we knew that the 2-L ferrihydrite adsorbent itself basically had a strong adsorption affinity. Although the 2-L ferrihydrite adsorbent is saturated by the phosphate ions, the pores were not noticeably clogged after the phosphate adsorption compared to before, as shown in Fig. 6(a) and (b). This means that the phosphate adsorption occurred by way of monolayer adsorption in the mesoporous pores of the 2-L ferrihydrite adsorbent.

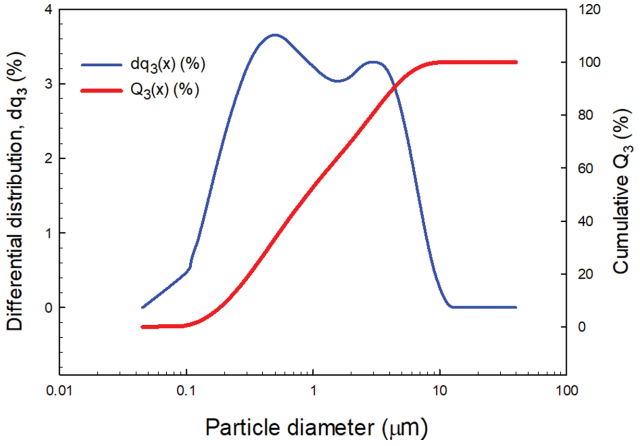

Fig. 7. Particle size distribution of synthesized 2-L ferrihydrite.

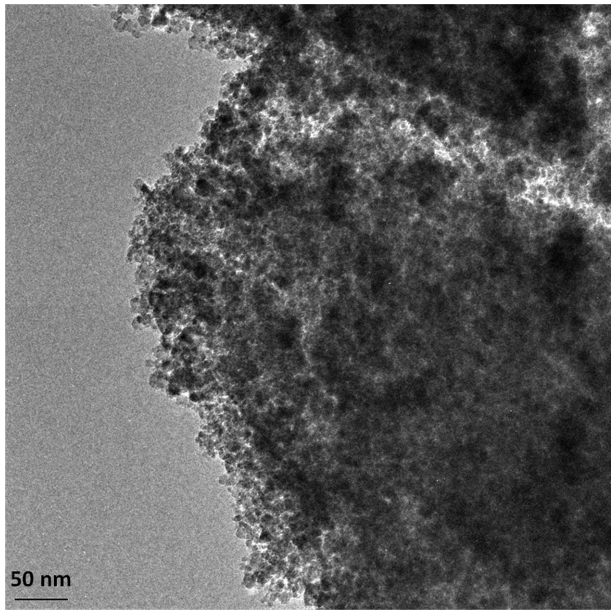

Fig. 8. TEM image of 2-L ferrihydrite particles.

Fig. 7 shows the particle size distribution of the synthesized 2-L ferrihydrite particles. The particle sizes were demonstrated by the dual-modal size distribution in the range of 0.1-10 μm.

Fig. 8 shows the TEM image of 2-L ferrihydrite particles. In preparation for the analysis of the internal microstructure of the particles, bulky 2-L ferrihydrite particles were milled to an average particle size of 200 nm by a planetary mill machine. The TEM image shows that the 2-L ferrihydrite adsorbent has a mesoporous structure aggregated by primary particles.

1. Partial Charge Modelling Part

The basic premise of the partial charge model is that the surface charge of a solid particle is highly influenced by the characteristics of the surrounding solution, such as its acidity or alkalinity. As described above, two possible models have thus far been proposed as the influential crystal structure of 2-L ferrihydrite: an exclusively octahedral structure and a combined tetrahedral (20%) and octahedral (80%) structure.

Table 4. Calculated partial charges of 2-L ferrihydrite with an octahedral structure for acidic and alkaline conditions

Octahedral formula	$\overline{\chi}$	δ(Fe)	δ(OH)
$[FeO(OH)\cdot(H_3O)_4]^{+4}$	+2.845	+0.631	+0.060
$[FeO(OH)\cdot(H_2O)_1\cdot(H_3O)_3]^{+3}$	+2.776	+0.592	+0.029
$[FeO(OH)\cdot(H_3O)_2]^{+2}$	+2.699	+0.549	−0.005
$[FeO(OH)\cdot(H_2O)_1\cdot(H_3O)_1]^{+1}$	+2.612	+0.500	−0.044
$[FeO(OH)\cdot(H_2O)_2]^{0}$	+2.513	+0.445	−0.088
$[FeO(OH)_2\cdot(H_2O)_3]^{-1}$	+2.399	+0.381	−0.139
$[FeO(OH)_3\cdot(H_2O)_2]^{-2}$	+2.268	+0.307	−0.197
$[FeO(OH)_4\cdot(H_2O)_1]^{-3}$	+2.115	+0.221	−0.226
$[FeO(OH)_5]^{-4}$	+1.933	+0.119	−0.347

The partial charge of the 2-L ferrihydrite adsorbent was calculated by employing the partial charge model, which also enabled the pH to be varied. Then, the calculated result was compared with the experimental result.

For the exclusively octahedral structure, the partial charge of the surface hydroxyl groups, δ(OH), was revealed to have a maximal value of +0.060 under strongly acidic conditions.

Table 4 lists the calculated partial charges of the adsorbent with an exclusively octahedral structure for both acidic and alkaline conditions. In the octahedral structure, the four water molecules coordinated in the crystal structure can be replaced by a maximum of four H_3O^+ molecules under acidic conditions. The partial charge depends on the degree of replacement, as indicated in Table 4. Under acidic conditions, δ(OH) of the 2-L ferrihydrite adsorbent has a maximal value of +0.060, higher than the value of 0.088 in the neutral state. The important finding is that δ(OH) becomes a positive value, the magnitude of which is determined by the degree of replacement of the adsorbed and structural water included in the crystal by hydronium ions (H_3O^+) from the acidic electrolyte. Under alkaline conditions, the value of δ(OH) was lower at −0.347. The negative value indicates that the surface of the adsorbent would repel the negative phosphate adsorbed on the adsorbent because of the existence of a repulsive force. Accordingly, we confirmed, a positive charge would allow the adsorbent to easily adsorb a negatively charged adsorbate such as phosphate under acidic conditions. The adsorbate could subsequently be desorbed from the surface of the adsorbent in a strongly alkaline solution.

Table 5 presents the partial charges of the combined tetrahedral (20%) and octahedral (80%) structure under acidic and alkaline conditions. For the combined structure, δ(OH) has a maximal value of +0.056 under acidic conditions and a value of −0.087 in the neutral state. Under alkaline conditions, δ(OH) reached a minimum value of −0.332. Ultimately, the adsorbent with the octahedral structure has a larger adsorption force than the combined structure. That is, a crystal structure with a higher coordination number is shown to be a more effective adsorbent.

2. Adsorption Experimental Part

Traditionally, the evaluation of the adsorption characteristics such as the adsorption mechanism and the adsorption capacity was mainly by conducting adsorption experiments. However, as indicated by the results obtained with the partial charge model described above, we could predict the adsorption and desorption phenomena of phosphate by calculating the partial charge of the adsorbent for various pH levels.

Fig. 9 illustrates the phenomenon of adsorption and desorption of phosphate on the 2-L ferrihydrite adsorbent under acidic and alkaline conditions. The adsorption force is affected by the basic adsorption affinity of the adsorbent plus the amount of adsorption as determined by the pH level.

The results of the BET analysis indicated that the 2-L ferrihydrite material is mesoporous with a strong adsorption affinity; furthermore, the adsorption force is determined by the amount of adsorption of 50 mg/g, affected by the PZC. The surface charge of the adsorbent has a positive value under acidic conditions based on the PZC, in which case the negative phosphate ion is strongly adsorbed on the positive surface of the adsorbent and the adsorbed amount reaches a maximum. In this adsorption experiment, the maximum amount adsorbed was 173.40 mg/g.

Under alkaline conditions, the surface charge of the adsorbent has a negative value because the pH is larger than the PZC value. In this case, the negative phosphate ion is gradually desorbed from the negative surface of the adsorbent and the amount of adsorption reaches a minimum. In this adsorption experiment, the minimum amount adsorbed was 28 mg/g. If the repulsive force of the adsorbate-adsorbent exceeds the adsorption force of the adsorbent itself of the PZC, the adsorbent will not adsorb the phosphate and the adsorbed phosphate will be desorbed conversely.

Table 5. Calculated partial charges of 2-L ferrihydrite with a combined tetrahedral (20%) and octahedral (80%) structure under acidic and alkaline conditions

Combined molecular formula	$\overline{\chi}$	δ(Fe)	δ(OH)
$(FeO(OH)\cdot(H_3O)_2)^{+2}$ (20%)+$FeO(OH)\cdot(H_3O)_4)^{+4}$ (80%)	+2.836	+0.626	+0.056
$(FeO(OH)\cdot(H_3O)_2]^{+2}$ (20%)+$(FeO(OH)\cdot(H_2O)_1\cdot(H_3O)_3)^{+3}$ (80%)	+2.781	+0.595	+0.031
$(FeO(OH)\cdot(H_3O)_2)^{+2}$ (20%)+$(FeO(OH)\cdot(H_2O)_2\cdot(H_3O)_2)^{+2}$ (80%)	+2.719	+0.561	+0.004
$(FeO(OH)_2\cdot(H_2O)_1\cdot(H_3O)_1)^{+1}$ (20%)+$(FeO(OH)\cdot(H_2O)_3\cdot(H_3O)_1)^{+1}$ (80%)	+2.625	+0.514	−0.033
$(FeO(OH)\cdot(H_2O)_2)^{0}$ (20%)+$(FeO(OH)\cdot(H_2O)_4)^{0}$ (80%)	+2.515	+0.446	−0.087
$(FeO(OH)_2\cdot(H_2O)_1)^{-1}$ (20%)+$(FeO(OH)_2\cdot(H_2O)_3)^{-1}$ (80%)	+2.387	+0.374	−0.145
$(FeO(OH)_3)^{-2}$ (20%)+$(FeO(OH)_3\cdot(H_2O)_2)^{-2}$ (80%)	+2.234	+0.288	−0.212
$(FeO(OH)_3)^{-2}$ (20%)+$(FeO(OH)_4\cdot(H_2O)_1)^{-3}$ (80%)	+2.111	+0.219	−0.236
$(FeO(OH)_3)^{-2}$ (20%)+$(FeO(OH)_5)^{-4}$ (80%)	+1.966	+0.137	−0.332

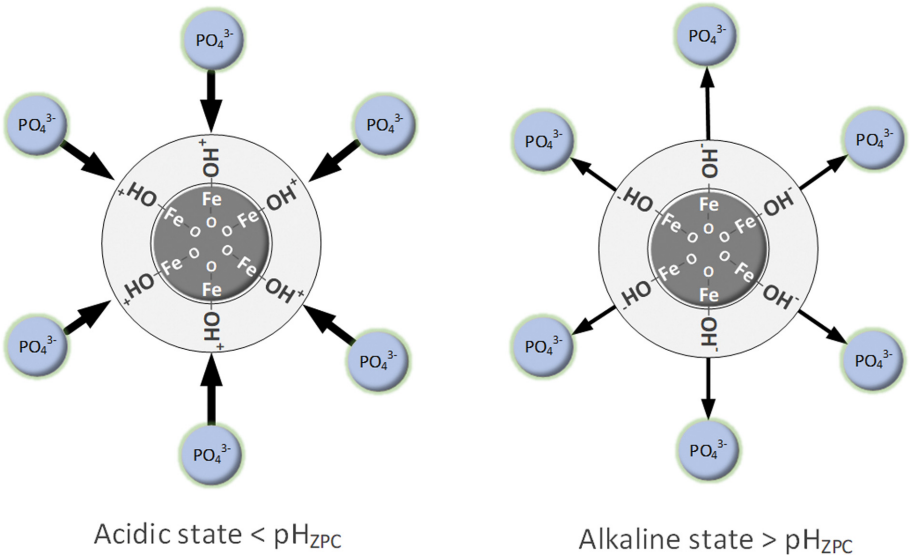

Fig. 9. Schematic diagram of the adsorption and desorption mechanisms of phosphate from the 2-L ferrihydrite adsorbent under acidic and alkaline conditions.

In the result obtained with the PCM model, the surface charge of the 2-L ferrihydrite in the neutral state was found to have values in the range of –0.088 to –0.087. Although the phosphate ion is negative, it is adsorbed on the negatively charged surface of the adsorbent because the basic adsorption affinity of the 2-L ferrihydrite adsorbent can overcome the negative surface charge.

Ultimately, a material with a stronger adsorption affinity is a good adsorbent. The optimal operating conditions under which the amount of adsorption is maximized must be determined by optimizing the pH.

In the acidic state in which the pH is less than pH_{ZPC}, the total adsorption force rapidly strengthens as a result of the strong adsorption affinity of the mesoporous 2-L ferrihydrite adsorbent itself plus the positively charged surface. Accordingly, the negative phosphate ion is adsorbed on the surface of the adsorbent to the maximum amount. Under alkaline conditions under which the pH is larger than pH_{ZPC}, the total adsorption force is determined by the strong adsorption affinity of the mesoporous 2-L ferrihydrite adsorbent itself minus the adsorption force of the negatively charged surface. Finally, in the alkaline state, the adsorbed phosphate is desorbed from the surface of the adsorbent as a result of the weak adsorption force, as shown in Fig. 9.

The 2-L ferrihydrite adsorbent is known to strongly interact with various types of cations and anions [1,41,42]. According to our calculations, cations would easily be adsorbed under alkaline conditions but, in contrast, the effective adsorption of anions would require acidic conditions.

Fig. 10 shows the PZC of the 2-L ferrihydrite adsorbent determined by EpHL, the measurement of the equilibrium pH at high surface loading [50,51]. The results of these measurements showed the PZC value to be 5.2. This final pH value does not coincide with the initial pH value in Fig. 10. This phenomenon is governed by the intrinsic surface characterization of the adsorbent. This result means that the 2-L ferrihydrite adsorbent has a positive surface

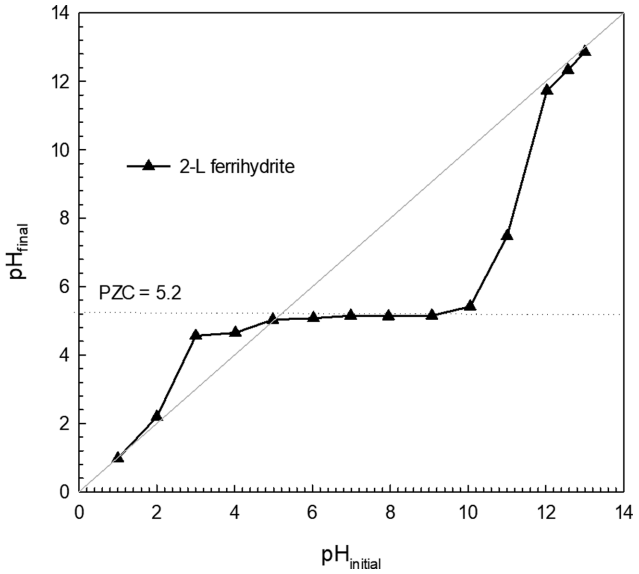

Fig. 10. PZC of the 2-L ferrihydrite adsorbent determined by EpHL measurements.

charge at pH<7, a negative surface charge at pH>10, and a charge of zero in the range of 7≤pH≤10.

This indicates that the zero charge of the adsorbent in the range of 7≤pH≤10 is caused by the intrinsic surface characterization of the adsorbent to enable it to compensate for the fluctuation in external charges.

Fig. 11 presents the amount of phosphate that was adsorbed under various pH conditions. As shown in Fig. 11, the maximum and minimum amounts that were adsorbed were experimentally found to be 173.40 mg/g at pH 5.0 and 28.80 mg/g at pH 13.0. This result indicates that the maximum amount adsorbed at pH 5.0 was six times higher compared with that at pH 13.0. Thus, ad-

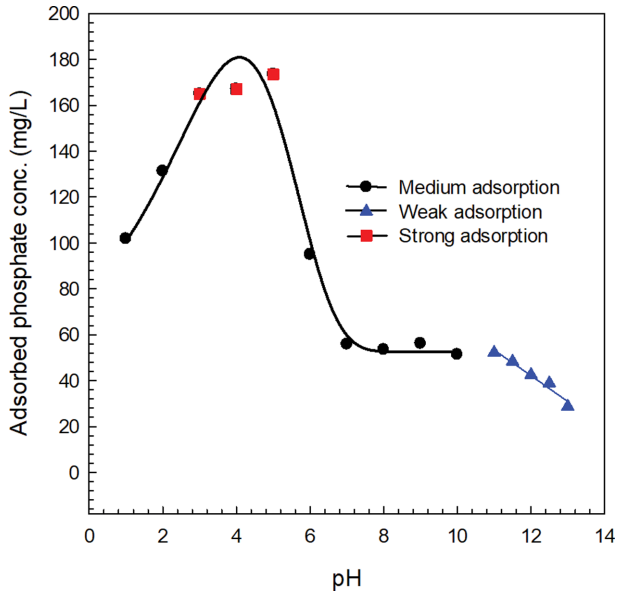

Fig. 11. Phosphate adsorption characteristics of the 2-L ferrihydrite adsorbent according to the pH levels.

Table 6. Efficiency of desorption of phosphate ions from the 2-L ferrihydrite adsorbent

pH_{des}	Maximum desorption conc. (mg/L)	Desorbed conc. (mg/L)	Desorption efficiency (%)
11.0	173.40	52.20	69.89
11.5	173.40	48.37	72.10
12.0	173.40	42.60	75.43
12.5	173.40	38.90	77.57
13.0	173.40	28.80	83.39

justment of the pH of the solution containing the 2-L ferrihydrite adsorbent with the adsorbed phosphate from pH 5.0 to pH 13.0 lowered the amount of adsorbed phosphate from 173.40 mg/g to 28.80 mg/g.

The desorption efficiency was lowered from 69.89% at pH 11.0 to 83.39% at pH 13.0 owing to the rapid decrease in the adsorption ability resulting from the increase in the pH under strongly alkaline conditions, as shown in Table 6. This means that the adsorbent could be regenerated to 83.39% of virgin adsorbent at pH 13.0.

Under acidic conditions, the amount of phosphate adsorbed to the charged surface of the adsorbent increases as the pH decreases. Accordingly, the negative phosphate ion is easily adsorbed onto the surface of the adsorbent.

On the other hand, the negative surface charge of the adsorbent was decreased by increasing the pH in the alkaline range. As a result, the negative phosphate adsorbate could easily be desorbed from the negatively charged adsorbent. However, the maximal adsorption behavior of the 2-L ferrihydrite adsorbent towards phosphate occurred at pH 3 to 5, whereas the adsorbed amount decreased at pH levels below 3. The maximal adsorption force in the range pH 3 to 5 means that the water molecules included in the adsorbent were entirely replaced by H_3O^+ ions of the acidic electrolyte and the positive surface charge of the adsorbent attained the maximal value.

Conversely, the adsorption force rapidly weakened below pH 3. Commonly, phosphate ions dissolve in the form of HPO_4^{2-}, $H_2PO_4^-$, and PO_4^{3-} in aqueous solution. The predominant species of phosphate that form at a given pH level are as follows: PO_4^{3-} ion at pH>12.2, HPO_4^{2-} ion at 7.2<pH<12.2, $H_2PO_4^-$ ion at 2.1<pH<7.2 and H_3PO_4 at pH<2.1. These forms of phosphate indicate that the phosphate ion exists as H_3PO_4 at pH<2.1 [52]. Accordingly, the rapid decrease in the amount of adsorption at pH<3 in this experiment is caused by the formation of stable H_3PO_4 and the anionic effect of an excessively acidic electrolyte. As a result, the adsorption force rapidly and adversely weakens under strongly acidic conditions below pH 3.

Meanwhile, under strongly alkaline conditions above pH 10, the adsorption force weakens as the pH increases. This is caused by the increasingly negative surface charge of the adsorbent as calculated with the partial charge model in Tables 4 and 5. The overall conclusion is that the optimal pH conditions for maximum adsorption exist in the range of 3≤pH≤5.

To determine the pH level that enables the maximum amount of adsorption in the acidic range, we compared the results of the partial charge model with the experimental data shown in Fig. 11. Under alkaline conditions, the adsorption ability gradually decreased from pH 11 to 13, and the minimal adsorption capacity appeared at pH 13. This means that the phosphate is desorbed because the limited adsorption amount decreases as a consequence of the increasingly negative surface charge of the adsorbent.

CONCLUSIONS

The chemical adsorption behavior of the adsorbate (phosphate) on the adsorbent (2-L ferrihydrite) was predicted by calculating the surface charge of the adsorbent by using the partial charge model and by varying the pH level in the range pH 1-13.

The crystal structure of the 2-L ferrihydrite was considered to be an exclusively octahedral model and a combined tetrahedral (20%) and octahedral (80%) model. For the exclusively octahedral model, the surface charges calculated by the partial charge model indicated that the δ(OH) of the surface reached a maximal value of +0.060 in the acidic state, a value of −0.088 in the neutral state, and a minimal value of −0.347 in the strongly alkaline state. For the combined model comprising 20% tetrahedra and 80% octahedra, the maximal value of δ(OH) was +0.056 in the acidic state, with values of −0.087 and −0.332 under neutral and strongly alkaline conditions, respectively.

Irrespective of the structural model used in the calculation, these surface charges enabled an effective interpretation of the adsorption and desorption phenomena of the anionic phosphate ion on the 2-L ferrihydrite adsorbent.

The surface charge of the adsorbent could be adjusted to become positive or negative by varying the pH of the solution. In an acidic solution of which the pH is less than 6, the negative phosphate ion is readily adsorbed because the δ(OH) of the adsorbent has a positive value. In contrast, under alkaline conditions above pH 10, the

adsorption force rapidly weakened, and the adsorbed phosphate ion was readily desorbed from the adsorbent because δ(OH) has a negative value under these conditions. This result of the partial charge model was also well consistent with the results of the adsorption experiment.

In conclusion, our study shows that the phenomena of chemical adsorption and desorption of an adsorbate on an adsorbent under various pH conditions can be theoretically predicted by using the partial charge model to calculate the surface charge value.

ACKNOWLEDGEMENTS

This research was supported by the Basic Science Research Program through the National Research Foundation of Korea (NRF) funded by the Ministry of Education (Project No.: 2019R1I1A1 A01041329). FE-TEM experiments were carried out on the Tecnai, Thermo system (in KBSI Seoul Center) and ICP-MS measurement was conducted on the Agilent 7700s (in KBSI Daegu Center).

NOMENCLATURE AND UNITS

k : a constant that depends on the electronegativity scale
p_i : the stoichiometry of the *i*th atom in the compound
Z : the total charge of the ionic species

Greek Letters

δ_i : partial charge of an atom
χ_i : electronegativity of an atom
χ_i^o : electronegativity of a neutral atom
$\overline{\chi}_{AB}^o$: mean electronegativity
η : hardness

REFERENCES

1. Y. Feng, D. Zhao, S. Qiu, Q. He, Y. Luo, K. Zhang and S. Shen, *ACS Omega*, **6**, 33046 (2021).
2. P. Xia, X. Wang, X. Wang, J. Zhang, H. Wang, J. Song, R. Ma, J. Wang and J. Zhao, *J. Chem. Eng. Data*, **62**, 226 (2017).
3. M. Chen, C. Huo, Y. Li and J. Wang, *ACS Sustainable Chem. Eng.*, **4**, 1296 (2016).
4. P. Wang, L. Li, Y. Tian, L. Sun, W. Zhan, S. Chen, J. Zhang and W. Zuo, *Sci. Total Environ.*, **809**, 152124 (2022).
5. Y. Sun, X. Feng and W. Zheng, *J. Chem. Eng. Data*, **65**, 4512 (2020).
6. X. Yang, Y. Wei, Y. Jiang, Y. Wang, L. Chen, L. Peng, S. Zhang, Y. Yan and Y. Yan, *Ind. Eng. Chem. Res.*, **60**, 5352 (2021).
7. N. Kataria and V. K. Garg, *Chemosphere*, **208**, 818 (2019).
8. M. Naushad, T. Ahamad, A. A. Khalid, A. H. Al-Muhtaseb, G. E. Eldesoky and A. A. Khan, *Compos. Part B*, **172**, 179 (2019).
9. J. D. Kubicki, N. Kabengi, M. Chrysochoou and N. Bompoti, *Geochem. Trans.*, **19**, 8 (2018).
10. A. A. Mamuna, M. Moritaa, M. Matsuokab and C. Tokorob, *J. Hazard. Mater.*, **334**, 142 (2017).
11. L. Tian, Y. Liang, Y. Lu, L. Peng, P. Wu and Z. Shi, *Soil Sci. Soc. Am. J.*, **82**, 96 (2018).
12. S.-O. Kim, W. C. Lee, H. G. Cho, B.-T. Lee, P.-K. Lee and S. H. Choi, *Environ. Technol.*, **35**, 251 (2014).
13. S.-J. Yoo, *Korean J. Chem. Eng.*, **38**, 326 (2021).
14. L. Tian, Z. Shi, Y. Lu, A. C. Dohnalkova, Z. Lin and Z. Dang, *Environ. Sci. Technol.*, **51**, 10605 (2017).
15. N. P. Funnell, M. F. Fulford, S. Inoue, K. Kletetschka, F. M. Michel and A. L. Goodwin, *Commun. Chem.*, **3**, 1 (2020).
16. C. J. Masina, J. H. Neethling, E. J. Olivier, S. Manzini, L. Lodya, V. Srot and P. A. van Aken, *RSC Adv.*, **5**, 39643 (2015).
17. D. Carta, M. F. Casula, A. Corrias, A. Falqui, G. Navarra and G. Pinna, *Mater. Chem. Phys.*, **113**, 349 (2009).
18. S. V. Stolyar, D. A. Balaev, A. A. Krasikov, A. A. Dubrovskiy, R. N. Yaroslavtsev, O. A. Bayukov, M. N. Volochaev and R. S. Iskhakov, *J. Supercond. Novel Magn.*, **31**, 1133 (2018).
19. A. Manceau, *Earth Space Chem.*, **3**, 1576 (2019).
20. F. Mailot, G. Morin, Y. Wang, D. Bonnin, P. Ildefonse, C. Channe and G. Calas, *Geochim. Cosmochim. Acta*, **75**, 2708 (2011).
21. D. G. Rancourt and J.-F. Meunier, *Am. Mineral.*, **93**, 1412 (2008).
22. A. Manceau and W. P. Gates, *Clays Clay Miner.*, **45**, 448 (1997).
23. V. A. Drits, B. A. Sakharov, A. L. Salyn and A. Manceau, *Clay Miner.*, **28**, 185 (1993).
24. T. Hiemstra, *Geochim. Cosmochim. Acta*, **105**, 316 (2013).
25. R. M. Cornell and U. Schwertmann, *The iron oxides: structure, properties, reactions, occurrences, and uses*, Wiley-VCH, Weinheim (1996).
26. H. Camos-Pereira, D. B. Kleja, C. Sjöstedt, L. Ahrens, W. Klysubun and J. P. Gustafsson, *Environ. Sci. Technol.*, **54**, 15722 (2020).
27. B. Wu and I. M. C. Lo, *Environ. Sci. Technol.*, **54**, 4601 (2020).
28. T. Suratwala, R. Steele, P. E. Miller, L. Wong, J. F. Destino, E. Feigenbaum, N. Shen and M. Feit, *J. Am. Ceram. Soc.*, **102**, 1566 (2019).
29. I. S. Martakov, O. G. Shevchenko, M. A. Torlopov, E. Y. Gerasimov and P. A. Sitnikov, *J. Inorg. Biochem.*, **199**, 110782 (2019).
30. R. Mendoza-Serna, *J. Porous Mater.*, **10**, 31 (2003).
31. K. T. Ranjit, I. Martyanov, D. Demydov, S. Uma, S. Rodrigues and K. J. Klabunde, *J. Sol-Gel Sci. Technol.*, **40**, 335 (2006).
32. J. Livage, M. Henry and C. Sanchez, *Prog. Solid State Chem.*, **18**, 259 (1988).
33. J. D. Mackenzie and D. R. Ulrich, *Ultrastructure processing of advanced ceramics*, Wiley, New York (1988).
34. G. A. Klopman, *J. Am. Chem. Soc.*, **86**, 1463 (1964).
35. R. G. Pearson, *J. Org. Chem.*, **54**, 1423 (1989).
36. Y. Kobayashi, K. Fukushi and S. Kosugi, *Environ, Sci. Technol.*, **54**, 2304 (2020).
37. A. S. Barnard and H. Guo, *Nature's nanostructures*, Pan Stanford Publishing, Singapore (2012).
38. J. L. Jambor and J. E. Dutrizac, *Chem. Rev.*, **98**, 2549 (1998).
39. F. M. Michel, L. Ehm, S. M. Antao, P. L. Lee, P. J. Chupas, G. Liu, D. R. Strongin, M. A. A. Schoonen, B. L. Phillips and J. B. Parise, *Science*, **316**, 1726 (2007).
40. O. Sadeghi, L. N. Zakharov and M. Nyman, *Science*, **316**, 1359 (2015).
41. S. J. Smith, K. Page, H. Kim, B. J. Campbell, J. Boerio-Goates and B. F. Woodfield, *Inorg. Chem.*, **51**, 6421 (2012).
42. M. Shi, X. Min, Y. Ke, Z. Lin, Z. Yang, S. Wang, N. Peng, X. Yan, S. Luo, J. Wu and Y. R. Wei, *Sci. Total Environ.*, **752**, 141930 (2021).
43. T. Hiemstra, *Environ. Sci. Nano*, **6**, 752 (2018).
44. B.-S. Zhu, Y. Jia, Z. Jin, B. Sun, T. Luo and L.-T. Kong, *RSC Adv.*, **5**, 84389 (2015).
45. K. Rout, M. Mohapatra and S. Anand, *Dalton Trans.*, **41**, 3302

(2012).
46. F. Frau, D. Addari, D. Atzel, R. Biddau, R. Cidu and A. Rossi, *Water Air Soil Pollut*, **205**, 25 (2010).
47. X. Zhang, Y. Chen, N. Zhao, H. Liu and Y. Wei, *RSC Adv.*, **4**, 21575 (2014).
48. D. E. Janney, J. M. Cowley and P. R. Buseck, *Clays Clays Miner.*, **48**, 111 (2000).
49. H. F. Chappell, W. Thom, D. T. Bowron, N. Faria, P. J. Hasnip and J. J. Powell, *Phys. Rev. Mater.*, **1**, 036002-1 (2017).
50. M. D. Donohue and G. L. Aranovich, *Adv. Colloid Interface Sci.*, **76-77**, 137 (1998).
51. J. R. Regalbuto, *Catalyst preparation science and engineering*, CRC Press, New York (2007).
52. R. Richards, *Surface and nanomolecular catalysis*, CRC Press, New York (2006).
53. B. Saha, R. Bains and F. Greenwood, *Sep. Sci. Technol.*, **40**, 2909 (2005).